Biosensors and Bioelectronics 77 (2016) 330–338

Contents lists available at ScienceDirect

Biosensors and Bioelectronics

journal homepage: www.elsevier.com/locate/bios

A photoelectrochemical biosensor for fibroblast-like synoviocyte cell using visible light-activated NCQDs sensitized-ZnO/$CH_3NH_3PbI_3$ heterojunction

Xuehui Pang [a], Yong Zhang [a], Jihong Pan [b], Yanxia Zhao [c], Yao Chen [d], Xiang Ren [a], Hongmin Ma [a,*], Qin Wei [a,*], Bin Du [a]

[a] Key Laboratory of Chemical Sensing & Analysis in Universities of Shandong, School of Chemistry and Chemical Engineering, University of Jinan, Jinan 250022, China
[b] Shandong Medicinal Biotechnology Centre, the Key Lab for Biotechnology Drugs of Ministry of Health, The Key Lab of Rare and Uncommon Disease, Jinan 250022, China
[c] Shandong Academy of Medical Science Graduate Education Center, Jinan 250062, China
[d] School of Chemistry and Chemical Engineering, Shandong University, Jinan 250100, China

ARTICLE INFO

Article history:
Received 14 July 2015
Received in revised form
19 September 2015
Accepted 21 September 2015
Available online 25 September 2015

Keywords:
FLS
Cell
PEC
ZnO/$CH_3NH_3PbI_3$/NCQDs
Nanocomposites

ABSTRACT

Based on ZnO nanorods (NRs)/$CH_3NH_3PbI_3$/nitrogen-doped carbon quantum dots (NCQDs) nanocomposites, the highly sensitive detection of fibroblast-like synoviocyte (FLS) cell was realized by a photoelectrochemical (PEC) biosensor. ZnO/$CH_3NH_3PbI_3$/NCQDs nanocomposites were exploited as the photo-to-electron generator to produce the signal. $CH_3NH_3PbI_3$ was spin-coated on ZnO surface after ZnO NRs grew on ITO electrode then by dropping on the modified electrode, NCQDs were diffused and adhered to the surface of ZnO and $CH_3NH_3PbI_3$. In the presence of EDC/NHS, the combination of $CH_3NH_3PbI_3$ and NCQDs was achieved by the carboxyl groups (–COOH) and amino groups ($–NH_2$) in the preparation process. Furthermore, the capture probe of FLS cell, CD95 antibody, can be anchored by –COOH and $–NH_2$ groups through EDC/NHS. The specific recognition between the antibody capture probes and cell targets gained high-sensitive detection for FLS cell for the first time. The developed biosensor showed a wide linear range from 1.0×10^4 cell/mL to 10 cell/mL and a low detection limit of 2 cell/mL. This kind of biosensor would provide a novel detection strategy for FLS cell.

1. Introduction

The inflammation of rheumatoid arthritis (RA), a systemic autoimmune disease, caused chronic inflammation of the rheumatoid synovium and hyperplasia of synovial fibroblasts. The chronic inflammation can erode adjacent cartilage and bone, and cause subsequent joint destruction (Sokka, 2003). Fibroblast-like synoviocyte (FLS) in the rheumatoid synovium from patients is aggressive and proliferative, attaches and invades the normal cartilage (Wang et al., 2014). Therefore, FLS plays a potent role in all aspects of the pathogenesis of RA and the detection of FLS is significant for the early warning of RA. However, to the best of our knowledge, no work has been done for the detection of FLS cell before. Here, a visible light induced photoelectrochemical (PEC) biosensor for FLS cell detection was developed. PEC is a newly developed high-sensitive method with low background current. Its detection signal needs the help of photo-to-electron mediums, that ZnO NRs, $CH_3NH_3PbI_3$ and nitrogen-doped carbon quantum dots (NCQDs) proposed in this work.

As known, one-dimensional ZnO NRs have been developed to obtain high PEC performance. ZnO NRs are widely used in ultraviolet sensors (Chang et al., 2011), nanogenerators (Wang and Song, 2006; Zang et al., 2014b), solar cells (Wang et al., 2006; Wang and Song, 2006) and chemical sensors (Ahmad et al., 2014; Chen et al., 2009; Cui et al., 2015; Gu et al., 2011; Sun et al., 2014a, b; Sun et al., 2013; Yin et al., 2015; Zhang et al., 2014). However, ZnO is a typical *n*-type semiconductor with a direct wide band gap of about 3.37 eV, and still suffered from the inefficient use of sunlight and an unstable nature. Then, compositing with narrow band gap photosensitizer material is a popular and effective strategy to promote the light-response of ZnO NRs. Herein, $CH_3NH_3PbI_3$ and NCQDs are introduced to improve the light-absorption ability of ZnO NRs.

NCQDs are the derivates of CQDs. In order to enhance PEC performance and induce an upward shift of the Fermi level, it is

* Corresponding authors. Fax: +86 531 8276 5969.
E-mail addresses: mahongmin2002@126.com (H. Ma), sdjndxwq@163.com (Q. Wei).

http://dx.doi.org/10.1016/j.bios.2015.09.047
0956-5663/

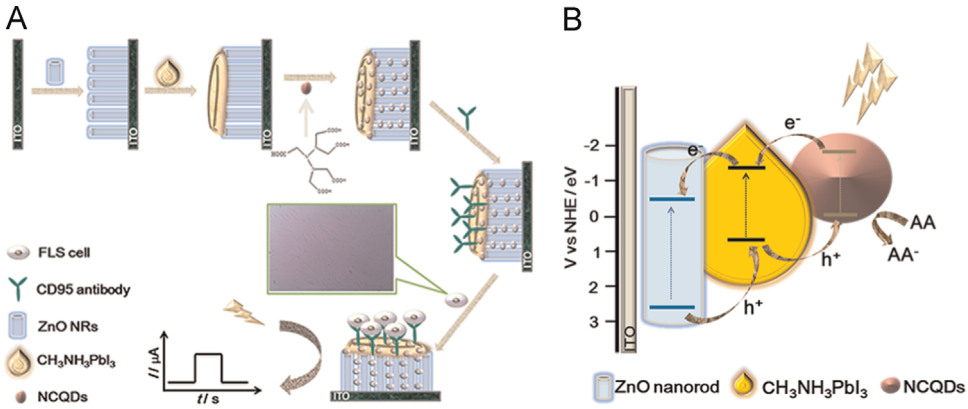

Scheme 1. (A) Schematic illustration of the PEC biosensor fabrication process and (B) schematic illustration of the energy level diagram.

suggested to dope nitrogen element in CQDs to produce –CN– and $–NH_2$ groups. The outstanding features of CQDs in the field of biosensing are their non-toxic and environmental friendly properties (Yang et al., 2009), therefore CQDs have been used in many fields of biosensing (Wang et al., 2013, 2015; Xu et al., 2013; Zhang et al., 2013; Zhou and Van Berkel, 1995), medical diagnosis (Pandey et al., 2013), catalysis (Li et al., 2013; Van Berkel and Zhou, 1995) and photovoltaic devices (Gupta et al., 2011) owing to its excellent properties (Hou et al., 2015; Zhao et al., 2013).

$CH_3NH_3PbI_3$ represents a novel class of light absorbing material. $CH_3NH_3PbI_3$ has high charge carrier mobility and long charge carrier life time, which suggests that the light-generated charges have long carrier transport lengths (Hodes, 2013). It is worth mentioning that $CH_3NH_3PbI_3$ can conduct not only positive holes but also electrons (Ball et al., 2013; Lee et al., 2012). Therefore, $CH_3NH_3PbI_3$ is selected as the sensitizer, which may provide a high-power conversion efficiency (Burschka et al., 2013).

Herein, a PEC biosensor for the detection of FLS cell was constructed as shown in Scheme 1(A). Photo-to-electron generator was the nanocomposite of ZnO NRs sensitized by NCQDs and $CH_3NH_3PbI_3$. The nanocomposites can enhance the adsorption of the visible light. Moreover, CD95 antibody was utilized to capture FLS cell. The detection mechanism was investigated and described in detail. The linear range and detection limit for FLS cell were studied. This PEC biosensor might offer a candidate method for FLS cell or other analytes.

2. Experimental

2.1. Regents

Phosphate buffered solution (PB, 0.067 mol/L KH_2PO_4 and 0.067 mol/L Na_2HPO_4) was used as the electrolyte for all PEC experiments. 0.1 mol/L KCl solution containing 5.0 mmol/L $K_3Fe(CN)_6/K_4Fe(CN)_6$ (1:1) was used as the electrolyte for all of EIS experiments. Pipette tips were sterilized for 40 min at 121 °C for later use. CD95 antibody was purchased from Shanghai Guyan technology Co. Ltd..

2.2. Apparatus

Scanning electron microscope (SEM) images were collected by JSM-6700F microscope (JEOL, Japan). Transmission electron microscope (TEM) images were collected by a transmission electron microscopy (JEOL, JEM-1400, Japan). High resolution transmission electron microscope (HRTEM) images were recorded by a JEM-2100F microscope (JEOL, Japan). X-ray diffraction (XRD) patterns were obtained from D8 focus diffractometer (Germany). Fourier transform infrared (FT-IR) spectra were collected by Perkin-Elmer 580B spectrophotometer (Perkin-Elmer, USA). Photoluminescence (PL) spectra were collected on LS-45/55 PL spectrometer (Perkin Elmer, USA). UV–vis measurements were performed on Lambda 35 UV–vis spectrometer (Perkin-Elmer, USA). Electrochemical impedance spectroscopy (EIS) and PEC tests were carried out on an electrochemical work station (Zahner Zennium PP211, Germany).

2.3. Preparation of ZnO NRs

ZnO NRs were prepared according to the literature (Pang et al., 2015a; Wang et al., 2010). Zinc acetate dehydrate (99.0%, Sinopharm Chemical Reagent Co., Ltd., China) was dissolved in the mixed solution with 2-methoxyethanol (AR, Sinopharm Chemical Reagent Co., Ltd., China) and ethanolamine (99.0%, Aladdin Industrial Inc., China). The concentrations of ethanolamine and $Zn(CH_3COO)_2$ (99.0%, Sinopharm Chemical Reagent Co., Ltd., China) were both 0.75 mol/L in the solution. The mixture was shaken for 30 min at 60 °C to produce a stable and uniform colloid solution. Half of ITO naked electrode was immersed into the colloid solution and ITO electrode was dried subsequently. Then the dried electrode was annealed for 10 min at 300 °C. The hydrothermal growth was performed at 95 °C in a stainless steel autoclave of 50 mL capacity with teflon liner. The modified electrode was immersed in 10 mL solution with 0.1 mol/L methenamine (99.5%, Aladdin Industrial Inc., China) and 0.1 mol/L $Zn(NO_3)_2$ (99.0%, Sinopharm Chemical Reagent Co., Ltd., China). Finally, the modified electrode was washed with ultrapure water (18.25 MΩ cm) and then dried in air. The duration of the growth process lasted for 4 h.

2.4. Preparation of NCQDs

NCQDs were prepared as the method described in the literature (Han et al., 2015). 10 g of DTPA were added into 100 mL ultrapure water and then stirred to generate a feculent solution. The formed solution was heated and then turned into colorless solution. The heating process was continued at 100 °C until a yellow clustered solid, namely NCQDs, was formed. The yellow solid was dissolved in 100 mL ultrapure water. Then, NCQDs solution was centrifuged for 15 min at 8000 r/min to eliminate the unreacted DTPA. Finally, the supernatant was freeze-dried to obtain the pure NCQDs solid.

2.5. Preparation of $CH_3NH_3PbI_3$

$CH_3NH_3PbI_3$ was prepared as in the literature (Kim et al., 2013) with slight modifications. 30 mL of methylamine (40% in methanol) and 30 mL of hydroiodic acid (57 wt% in water) were mixed and stirred for 2 h in the ice bath. The obtained solution was rotary evaporated at 50 °C until $CH_3NH_3I_3$ was precipitated. The

precipitate was washed with diethylether until becoming white, and then dried under vacuum for later use. 2.314 g (4 mL, > 99%) of PbI_2 (in γ-butyrolactone) and 0.79 g of the obtained $CH_3NH_3I_3$ reacted for 12 h at 60 °C under stirring.

2.6. Preparation of FLS cell

FLS cells were prepared according to our previous work (Wang et al. 2014). RA synovial tissue was finely chopped and incubated with type II collagenase (1 mg/mL, Sigma-Aldrich) in Dulbecco modified Eagle's medium (DMEM, HyClone, Thermo Scientific) for 6 h in a 37 °C, 5% CO_2 incubator (Thermo Scientific). FLS cells were filtered and cultured overnight in DMEM, and then supplemented with 10% fetal bovine serum (FBS, HyClone) as well as penicillin (100 IU/mL) and streptomycin (100 μg/mL, Gibco).

2.7. Fabrication of the PEC biosensor

The fabrication procedure of PEC biosensor was shown in Scheme 1(A). Firstly, ZnO nanorods grew on ITO electrode surface for 4 h after dropping three times in the reaction solution (part 2.2). Secondly, 11 μL of $CH_3NH_3PbI_3$ was spin-coated on ZnO/ITO electrode and annealed for 15 min at 300 °C. Thirdly, 6 μL of NCQDs (10 mg/mL) was dropped on $CH_3NH_3PbI_3$/ZnO/ITO electrode surface activated by EDC/NHS. After that, 10 μL of CD95 (30 μg/mL) marker antibody was dropped on NCQDs/$CH_3NH_3PbI_3$/ZnO/ITO electrode using an EDC/NHS and incubated in a 4 °C refrigerator for 4 h. At last, the different concentrations of FLS cells were dropped on CD95/NCQDs/$CH_3NH_3PbI_3$/ZnO/ITO electrode surface respectively and incubated at 4 °C for 4 h.

2.8. Measurement procedure

PEC measurements were performed immediately after the incubation of FLS cell. PEC and EIS experiments were operated at room temperature. A commercial LED light of 430 nm (180 W/m^2) was used as the irradiation energy in PEC tests. Electrolyte solution was PB containing 0.1 mol/L of ascorbic acid (AA). The bias voltage was 0.1 V. Light duration and no light duration were both 20 s. A three-electrode system was utilized in PEC and EIS tests, the working electrode was the modified ITO electrode, the reference electrode was a KCl-saturated calomel electrode (SCE), while the auxiliary electrode consisted of a platinum wire.

3. Results and discussion

3.1. Characterization of ZnO NRs, $CH_3NH_3PbI_3$ and NCQDs

3.1.1. The surface morphology characterization of ZnO NRs,

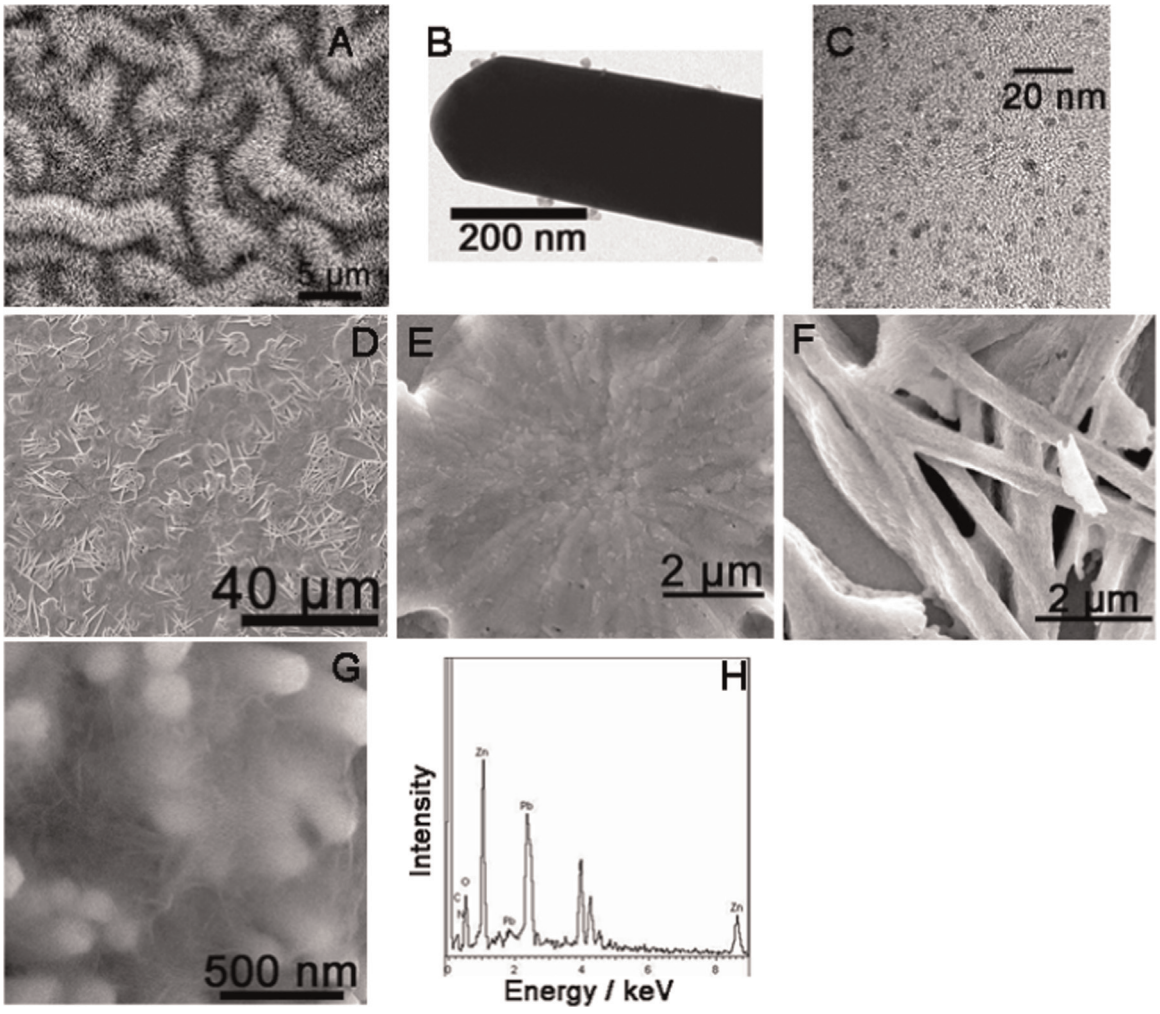

Fig. 1. SEM images of ZnO (A), $CH_3NH_3PbI_3$ (D, E, F) and ZnO/$CH_3NH_3PbI_3$/ NCQDs (G); TEM image of ZnO (B); HRTEM image of NCQDs (C); EDS of ZnO/$CH_3NH_3PbI_3$/ NCQDs (H).

$CH_3NH_3PbI_3$, NCQDs and ZnO/$CH_3NH_3PbI_3$/NCQDs

The morphology of as-prepared ZnO NRs was identified by SEM in Fig. 1A. Macroscopical picture showed ZnO NRs products. Fig. 1B displayed a low-magnification TEM image of a single ZnO NRs after growing on ITO and being scraped from the electrode. ZnO NRs showed the same contrast, which illustrated that ZnO crystals for composing ZnO NRs were almost identical.

The morphology and size of NCQDs were investigated by HRTEM in Fig. 1C. Many nearly spherical dots with an average diameter of 3~5 nm appeared in the visual field of HRTEM image. They were the prepared NCQDs with high volume of production. From HRTEM image, it can be deduced the preparation of NCQDs was successful.

Fig. 1D showed a macroscopical morphology of $CH_3NH_3PbI_3$. It can be seen that $CH_3NH_3PbI_3$ products looked like a dry pool filling with plenty of the "lotus leaves and branches" in general. Fig. 1E and F showed clear "lotus leaf and branch".

Fig. 1G showed the morphology for ZnO NRs/$CH_3NH_3PbI_3$/NCQDs. ZnO NRs can be dimly distinguished. A thin cover like gauze can be seen, which should be $CH_3NH_3PbI_3$ film. EDS result in Fig. 1H exhibited six elements of Zn, O, Pb, I, C and N in the sample, which further convinced the combination of ZnO NRs, $CH_3NH_3PbI_3$ and NCQDs was successful.

3.1.2. XRD characterization of ZnO NRs, $CH_3NH_3PbI_3$, NCQDs

Fig. 2A displayed XRD pattern of ZnO NRs. For ZnO NRs, 10 diffraction peaks can be distinguished as ordinal (100), (002), (101), (102), (110), (103), (112), (201), (004) and (202) lattice planes as reported (Wang et al., 2010). Fig. 2B presented XRD pattern of $CH_3NH_3PbI_3$. There were four peaks appeared, which were indexed to 14.1°, 28.3°, 31.9° and 43.0° for (110), (220), (310) and (330) lattice planes respectively (Burschka et al., 2013). Fig. 2C exhibited XRD pattern of NCQDs. There was a dispersed and weak diffraction peak (002) centering at $2\theta=23°$, showing a lattice spacing (d) of 0.385 nm. This d value was also larger than that of bulk graphite of about 0.34 nm along (002) direction (Peng et al., 2012). And also, this d value was consistent with that of the carbon nanoparticles of (002) lattice spacing (Dong et al., 2014).

3.1.3. FT-IR characterization of $CH_3NH_3PbI_3$ and NCQDs

Fig. 2D showed FT-IR spectra of $CH_3NH_3PbI_3$ and NCQDs in the wavenumber range of 500–4000 cm^{-1}. The above line corresponded to FT-IR spectrum of $CH_3NH_3PbI_3$. A weak peak at 3447 cm^{-1} was assigned to hydroxyl groups. The broad peaks in the range of 3010–3130 cm^{-1} corresponded to C–H bond stretching vibrations. The peak centered at 1650 cm^{-1} was associated to C–O band stretching vibrations and the sharp peak at 1401 cm^{-1} was ascribed to C=O bending vibration. The peak at 1146 cm^{-1} indicated the stretching vibrations of C–N bond. FT-IR results showed that $CH_3NH_3PbI_3$ had abundant amino and carboxyl groups. The bottom line referred to FT-IR spectrum of NCQDs. The presence of hydroxyl groups on NCQDs surfaces was proved by a broad peak centered at 3429 cm^{-1}. The wide peaks in the range of 3010–3140 cm^{-1} were assigned to C–H bond stretching vibrations. The peak at 1728 cm^{-1} indicated C=O stretching vibration. The peak centered at 1635 cm^{-1} might be ascribed to C–O band stretching vibrations. C=O bending vibration was at 1396 cm^{-1}. The peak at 1216 cm^{-1} suggested the characteristic stretch of C–N bond. FT-IR data indicated that NCQDs loaded lots of carboxyl groups and amino groups. The amino and carboxyl groups contained in $CH_3NH_3PbI_3$ and NCQDs would increase the hydrophilicity and biocompatibility for the detection target cell in aqueous system (Han et al., 2015). Moreover, these functional groups would benefit for integrating

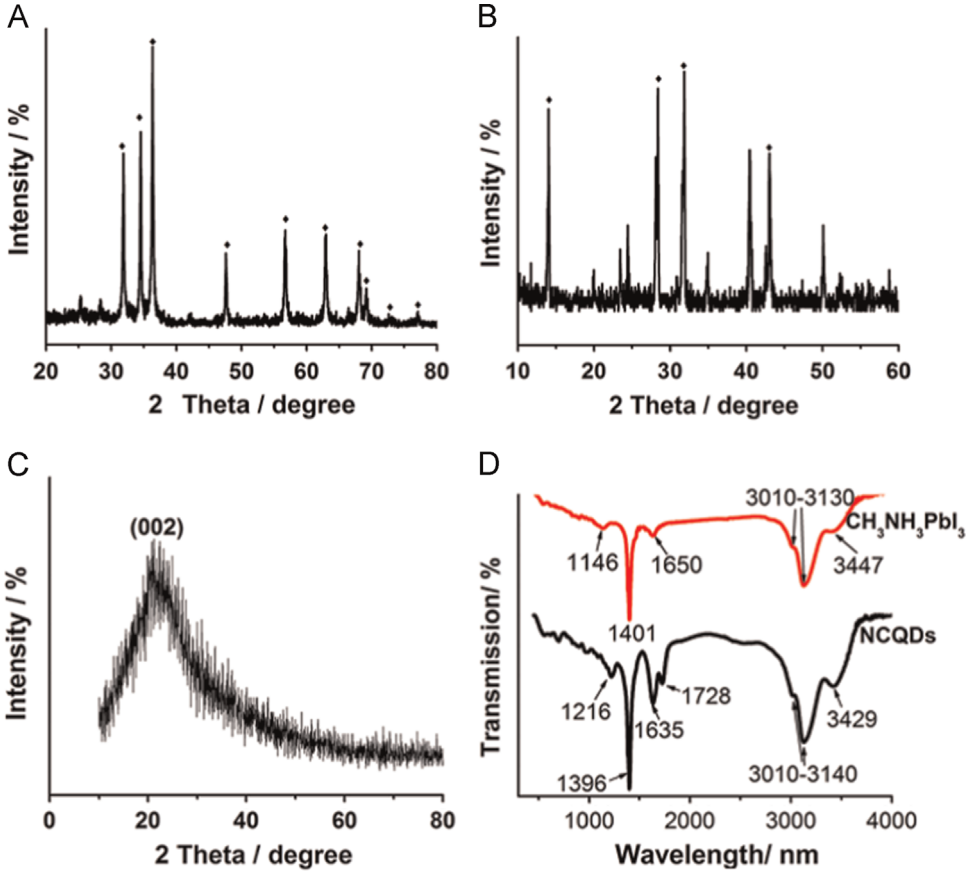

Fig. 2. XRD patterns of ZnO (A), $CH_3NH_3PbI_3$ (B) and NCQDs (C); FTIR spectra (D) of $CH_3NH_3PbI_3$ and NCQDs.

$CH_3NH_3PbI_3$ and NCQDs by the activation of EDC/NHS.

3.2. The proposed mechanism of PEC performance enhancement

A scheme of the energy level diagram was presented (Scheme 1 (B)). Electronic energy levels (EELs) of those substitute materials were needed to match EELs of the perovskite materials for efficient charge transfer. The conduction band (CB) of ZnO and $CH_3NH_3PbI_3$ were −0.5 eV (Pang et al., 2015a) and −1.34 eV (Liu et al., 2015) respectively. VB edge potential of NCQDs was about 0 eV (Narayanan et al., 2013). The band gap of ZnO, $CH_3NH_3PbI_3$ and NCQDs were about 3.37 eV, 2.2 eV (Stoumpos et al., 2013) and 1.9 eV (M. Sun et al., 2014), respectively. VB of ZnO and $CH_3NH_3PbI_3$ were 2.87 eV and 0.88 eV respectively and CB edge potential of NCQDs was about −1.9 eV (according to the formula $E_g = V_{VB} - V_{CB}$) (Pang et al., 2015a,b; Zang et al., 2014a). Thus, the components (ZnO, $CH_3NH_3PbI_3$ and NCQDs) formed type II heterojunctions with staggered band alignments, which facilitated the charge transfer during photocurrent conversion process. Upon visible light illumination, the weakly bound exciton and free charge carrier coexisted. The charge extraction and exciton dissociation were present based on NCQDs. The excitons in NCQDs dissociated at the $CH_3NH_3PbI_3$/NCQDs interface. No matter what the proportion of photogenerated free-charge carriers versus excitons generated upon illumination was, the injection of the electrons from NCQDs into $CH_3NH_3PbI_3$ occurred at $CH_3NH_3PbI_3$/NCQDs interface by charge extraction and/or exciton dissociation. Therefore, the excitons generated by NCQDs absorption injected into ZnO layer finally, but the simultaneously generated h^+ still remained in NCQDs layer. The excitons (generated by $CH_3NH_3PbI_3$) did not take vast dissociation inside the $CH_3NH_3PbI_3$ layer, and these excitons dissociated at $CH_3NH_3PbI_3$/ZnO interface. Therefore, most of the excitons (from $CH_3NH_3PbI_3$ and NCQDs) injected into ZnO and the holes injected into NCQDs. As a reducing agent, AA acted as an electron donor for trapping holes, which inhibited e^-/h^+ recombination and improved the photocurrent response (Gao et al.,

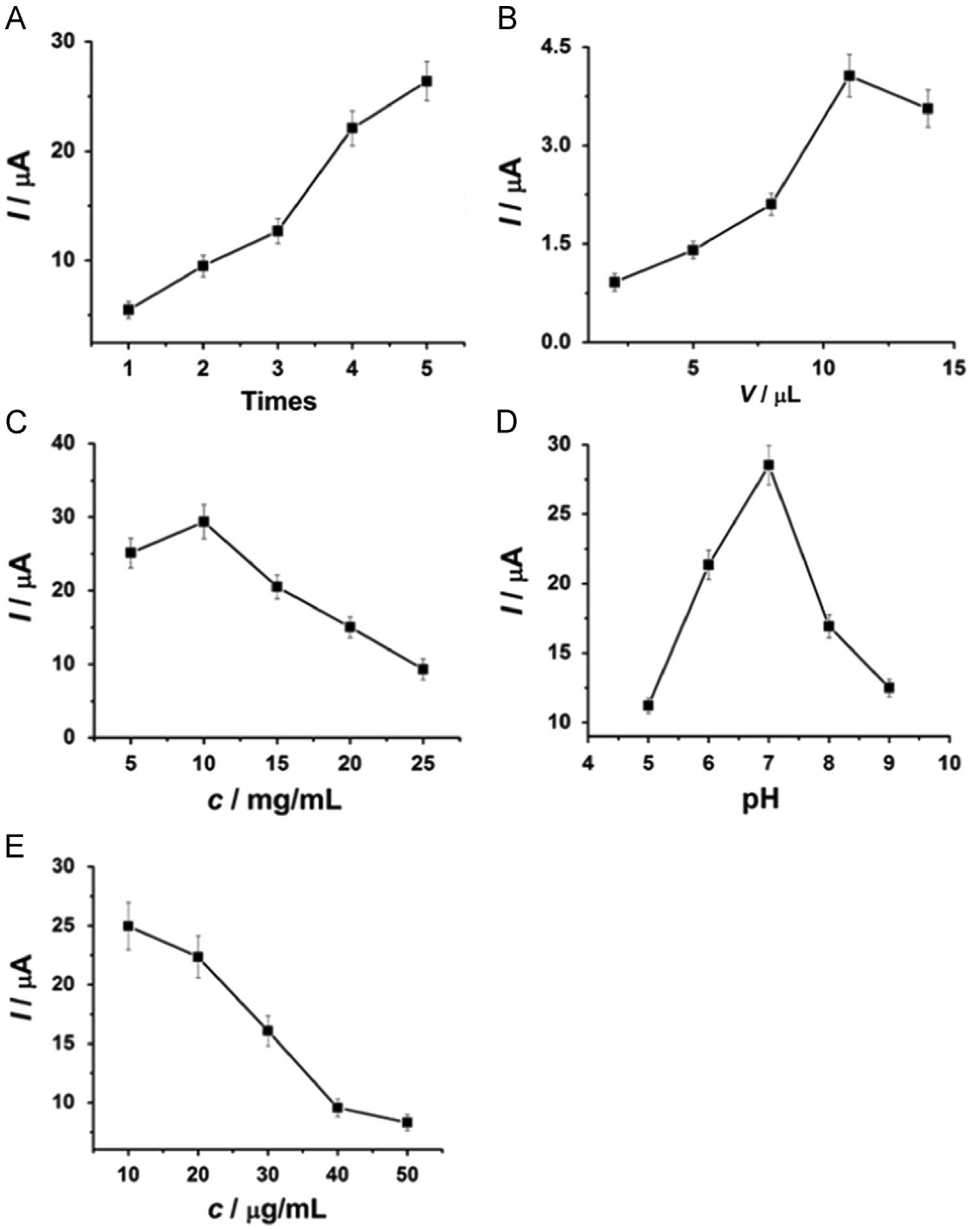

Fig. 3. The optimization of experimental conditions by time-based photocurrent responses of (A) the different drop times of ZnO NRs, (B) the different application amount of $CH_3NH_3PbI_3$, (C) the different concentration of NCQDs, (D) different pH after modifying ZnO (3 times)/$CH_3NH_3PbI_3$ (11 μL)/NCQDs (10 mg/mL, 6 μL), (E) the different concentration of CD95 (pH = 7.4).

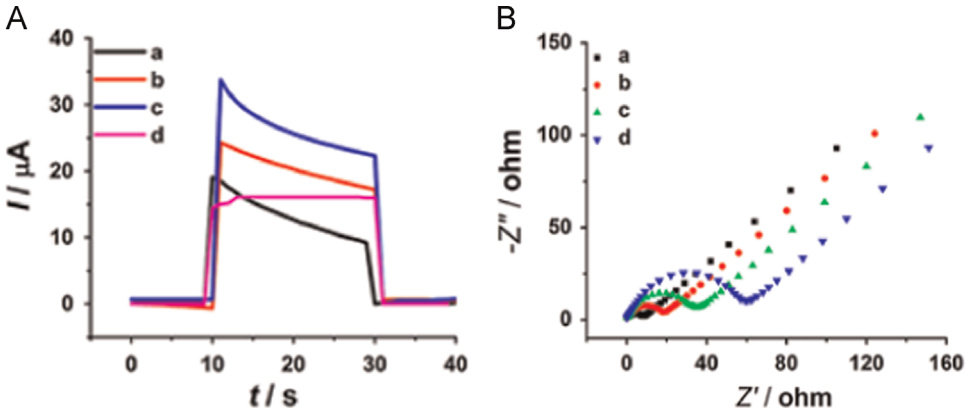

Fig. 4. Time-based photocurrent responses (A) and Nyquist plots (B) of (a) ZnO nanorods/ITO, (b) ZnO/$CH_3NH_3PbI_3$/ITO, (c) ZnO/$CH_3NH_3PbI_3$/NCQDs/ITO, (d) CD95/ZnO/$CH_3NH_3PbI_3$/NCQDs/ITO.

2015). After that, all of the photogenerated electrons and holes were transported toward ITO film and conducted through the external circuit to the counter electrode. So, ZnO acted as the main acceptor and transporter, $CH_3NH_3PbI_3$ and NCQDs served as the dominant light absorber, electron acceptor and electron transporter. The combination of ZnO, $CH_3NH_3PbI_3$ and NCQDs benefited for separating the charge and hindering e^-/h^+ recombination. The speculation was proved by PL characterization, PEC characterization, UV–vis characterization of ZnO NRs, ZnO NRs/$CH_3NH_3PbI_3$ and ZnO/$CH_3NH_3PbI_3$/NCQDs (ESI†, Fig. S1). Moreover, N-doping might be another factor for the enhancement of photocatalytic activity of ZnO/$CH_3NH_3PbI_3$/NCQDs. The reason might be that N-doping can decrease the work function of carbon nanomaterials.

3.3. Optimization of experimental conditions

It is well-known that experimental conditions affect PEC response. In order to obtain the best detection performance, the optimal experimental conditions were evaluated. The drop times of ITO electrode for ZnO NRs growth, the application amount of $CH_3NH_3PbI_3$, the concentration of NCQDs, pH values and the concentration of CD95 antibody were investigated (Fig. 3).

ZnO NRs played an important role in photo-to-electron conversion, which may have impact the integral property of the nanocomposites. Then the drop times of ITO electrode in the precursor solution was inspected. It can be seen from Fig. 3A, with increase of the drop times until reaching 5 times, the photocurrent went up monotonously. It might be the reason that the quantity of ZnO NRs produced more photo-to-electron generators and therefore promoted PEC ability. However, 3 times was selected as the optimal drop times for economical reason.

As mentioned above, $CH_3NH_3PbI_3$ had high charge carrier mobility and long charge carrier life time and can conduct not only positive holes but also electrons. The application amount of $CH_3NH_3PbI_3$ would affect PEC performance of the proposed biosensor. Then the application amount of $CH_3NH_3PbI_3$ was investigated (Fig. 3B). As shown, with the increasing application amount of $CH_3NH_3PbI_3$, the photocurrent response enhanced slowly up to 11 μL. Then the photocurrent dropped, which might be due to the further increased $CH_3NH_3PbI_3$ thickness suppressed the electron transfer. Thus, 11 μL of $CH_3NH_3PbI_3$ was used as the optimal application amount.

NCQDs were used as light harvesting material in this work. NCQDs possessed multiple exciton generation ability and the absorption ability of the different wavelength. So the concentration of NCQDs was studied (Fig. 3C). The photocurrent increased before reaching 10 mg/mL, which illustrated that NCQDs promoted the photocurrent conversion efficiency. But the photocurrent response fell down between 10 and 25 mg/mL. It might result from the inhibition from the excessive NCQDs. Thus, the optimal concentration of NCQDs was 10 mg/mL.

Too highly alkaline or acidic environment would affect the immobilization and bioactivity of FLS cell (Pang et al., 2015b), pH of PB was investigated in order to obtain the optimal PEC performance. Fig. 3D depicted the effect of pH on PEC current of the modified biosensor, which was carried out in PB with different pH from 5 to 9. The photocurrent response enhanced with increase pH in 5.0~7.0 but then decreased in high pH 7.0~9.0. The maximum photocurrent appeared at pH 7.0. This phenomenon explained the opinion that higher or lower pH would influence the bioactivity of the biomaterial and lead to a decrease in photocurrent response. Therefore, pH 7.0 was used as the optimal condition for the subsequent tests. Under the optimal pH, the proposed biosensor can achieve an optimal signal for the quantitative detection of FLS cell.

Considering the specific recognition effect between the capture probe CD95 antibody and FLS cell, PEC experiments were performed for the best immobilization affect as shown in Fig. 3E. The photocurrent dropped with increased concentration of CD95 antibody because this biomaterial could not transfer the electron and not absorb the light. What's more, the decrease of the photocurrent suggested that CD95 antibody were fixed by $CH_3NH_3PbI_3$ and NCQDs on the modified electrode. In consideration of the best immobilization affect and good PEC performance, the optimal concentration of CD95 antibody was 30 μg/mL.

3.4. Characterization of the fabricated PEC biosensor

The fabrication process was monitored by photocurrent responses under the optimal experimental condition (Fig. 4A). Curve a showed that the photocurrent remarkably enhanced after ZnO NRs grew on ITO electrode. When organic $CH_3NH_3PbI_3$ was spin-coated on ITO electrode, the photocurrent response enhanced about 5 μA (curve b). This indicated that the modification of $CH_3NH_3PbI_3$ conspicuously increased the photocurrent conversion efficiency. Subsequently, after NCQDs was modified, the photocurrent response improved up to about 33.8 μA (curve c). While exposed to the irradiation light, the electron transfer efficiency increased and the recombination probability between e^- and h^+ turned lower apparently because of the combination of ZnO, $CH_3NH_3PbI_3$ and NCQDs. This effective combination might make the electrons injection much easier between CB and VB and might be in favor of the enhancement of the biosensor sensitivity. Finally, when CD95 antibody was modified on the electrode, the photocurrent reduced obviously (curve d). Because of the modification and incubation, the interaction between –NH– and –COOH groups

of CD95 antibody and –NH– and –COOH groups of $CH_3NH_3PbI_3$ and NCQDs would occur under the activation of EDC/NHS. This chemical interaction made $CH_3NH_3PbI_3$ and NCQDs anchor CD95 antibody probe on ITO electrode successfully. But the antibody was composed mainly by organic amino acid molecular and these molecular were insulative. Then the amino acid molecular did not own the conductivity and visible light absorbency, resulting in the obstruction of the visible light absorption and the suppression of the electron. This speculation was proved by the photocurrent decrease of the experimental results. Therefore, the PEC biosensor was fabricated successfully.

EIS was carried out to assess the fabrication procedure of the biosensor under the optimal experimental conditions (Fig. 4B). The frequency range was from 50 mHz to 100 kHz with 5 mV amplitude. A Randles equivalent circuit illuminated Nyqusit plots (Jiang et al., 2013; Tsai et al., 2011) (ESI†, Fig. S2). R_s, namely the resistance of solution, represented the property of the electrolyte solution. Z_W, namely the Warburg impedance, represented the diffusion of the redox probe. Warburg curve in low frequency region related to the diffusion rate of the substance participating in the electrochemical redox reaction (Matsuzawa et al., 1998). Warburg resistance was controlled by the concentration polarization, which represented the speed of the mass diffusion. R_s and Z_W were not affected by the modified process. R_{et}, namely the charge transfer resistance, represented the resistance of the Faradic current of the fabricate process. Thus R_{et} was most significant

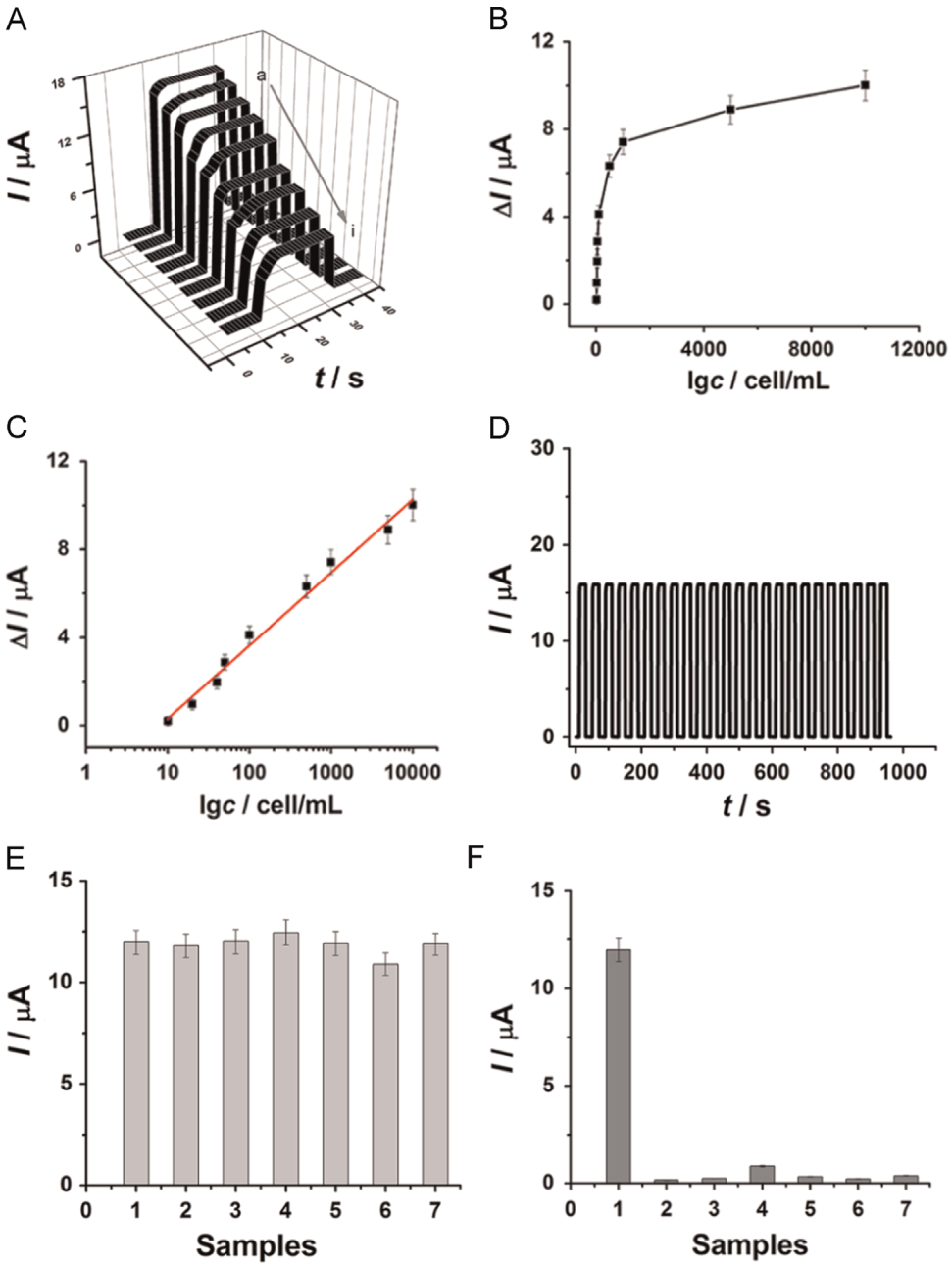

Fig. 5. Time-based photocurrent responses of (A) incubated with different concentrations of FLS cell; (B) Relation curve between photocurrent change (ΔI) and different FLS cell concentrations; (C) Logarithmic calibration curve between ΔI and concentration of FLS cell; (D) Stability of photocurrent response under the optimal condition; (E) Selectivity of the sensor (1) 100 cell/mL FLS cell; (2) 100 cell/mL FLS cell+200 cell/mL Saos-2 cell; (3) 100 cell/mL FLS cell+200 cell/mL endothelial cell; (4) 100 cell/mL FLS cell+200 cell/mL LNCaP cell; (5) 100 cell/mL FLS cell+200 cell/mL VCaP cell; (6) 100 cell/mL FLS cell+200 cell/mL Hela cell; (7) 100 cell/mL Saos-2/endothelial/LNCaP/VCaP/22RV1 cell; (F) Selectivity of the sensor (1) 100 cell/mL FLS cell; (2) 100 cell/mL Saos-2 cell; (3) 100 cell/mL endothelial cell; (4) 100 cell/mL LNCaP cell; (5) 100 cell/mL VCaP cell; (6) 100 cell/mL Hela cell and (7) 100 cell/mL Saos-2/endothelial/LNCaP/VCaP/ Hela cell.

among all of the impedance parameters. The values of R_{et} can be fitted by ZSimWin software. The semicircle in the high frequency region was controlled by the electrode activation. The sensor fabrication procedure was indicated by the semicircle portion (R_{et}) changes at high frequencies. R_{et} were 9 Ω, 18 Ω, 34 Ω and 59 Ω, corresponding respectively to curve a, b, c and d (Fig. 4B). Nyquist plot exhibited a small arc radius after growing ZnO NRs (curve a). Later on, the semicircle increased markedly when $CH_3NH_3PbI_3$ was modified, which might be attributed to the bad electrical conductivity (curve b). R_{et} value continuously increased after NCQDs was further modified electrode, suggesting that NCQDs depressed the electrical conductivity of the modified film (curve c). R_{et} increased significantly once CD95 antibody was modified because of the obvious insulation property (curve d). Consequently, the biosensor had been constructed effectively.

3.5. Analytical performance characteristics

To inspect the possibility of the biosensor to be applied for FLS cell detection, quantitative detection of FLS cell was handled under the determined optimal conditions. It can be seen in Fig. 5A and B, lower photocurrent responses were achieved with the increasing concentration of FLS cell. This indicated that the developed biosensor displayed good detection performance and can be used for FLS cell quantitative detection. A calibration graph was plotted under the optimum conditions (Fig. 5C) and a positive relationship was shown between the photocurrent response signal change (ΔI) and FLS cell target concentrations (c_{cell}). ΔI increased linearly with the logarithm of c_{cell} from 1.0×10^4 to 10 cell/mL. The linear equation was ΔI (μA) $= -3.277 + 3.438\ \lg c_{cell}$ (cell/mL) with a correlation coefficient of 0.994. A detection limit of 2 cell/mL was calculated for the proposed biosensor. The low detection limit may be attributed to good separated excitation energy, photocurrent conversion efficiency among ZnO, $CH_3NH_3PbI_3$ and NCQDs, and also attributed to the specific recognition between CD95 antibody and the cell target.

Reproducibility was an important parameter affecting the practical application of the sensor. Five biosensors were fabricated and used to determinate 500 cell/mL of FLS cell. The relative standard deviation (RSD) of 2.0% was obtained for FLS cell. Thus, the reproducibility of the proposed biosensor was good.

Stability was another important parameter influencing the practical application of the sensor. Fig. 5D indicated the photocurrent response of this PEC biosensor repeated per 20 s under the light irradiation (430 nm). In each on/off cycle, the photocurrent did not show any obvious change. The irradiation process was operated 24 on/off cycles over 900 s. It suggested that the photocurrent response was very stable and this strategy was suitable to fabricate PEC biosensors.

Selectivity is an important parameter in application of biosensor and the selectivity of biosensor was also investigated. Five other kinds of cells (Saos-2 cell, endothelial cell, LNCaP cell, VCaP cell, Hela cell) were used in this test. As shown in Fig. 5E, a fabricated biosensor incubated only with 100 cell/mL FLS cell was tested under the determined optimal conditions (sample 1). Five biosensors incubated with 100 cell/mL FLS cell containing 200 cell/mL Saos-2 cell, 200 cell/mL endothelial cell, 200 cell/mL LNCaP cell, 200 cell/mL VCaP cell, 200 cell/mL Hela cell respectively were also tested (samples 2–6). Sample 7 was the incubation of five other kinds of cells indicating the possible cross-reaction could be ignored. The photocurrent response was conformed to the calibration curve (100 cell/mL FLS cell).

To further inspect the selectivity, FLS cell-free sensors were tested as shown in Fig. 5F. Six FLS cell-free sensors (contained 100 cell/mL Saos-2 cell, endothelial cell, LNCaP cell, VCaP cell, Hela cell, the mixture respectively) were tested. As Fig. 5F shown, there was no conspicuous photocurrent change. And the sample 7 was the mixture of five kinds of cells indicating the selectivity was excellent.

To evaluate the performance of the biosensor, real samples were conducted in the Table S1 (ESI†). Real samples were tested to verify the precision by standard addition method. RSD were 1.71% and 1.80% for 105 cell/mL and 216 cell/mL respectively, and the recoveries were 102% and 98.8% respectively.

4. Conclusions

In this work, a novel, rapid and ultrasensitive PEC biosensor for FLS cell was fabricated. The signal generator of $ZnO/CH_3NH_3PbI_3$/NCQDs nanocomposites exhibited apparently enhanced PEC property. $CH_3NH_3PbI_3$ and NCQDs acted as the visible-light absorber, electron acceptor and transporter, their combination improving the charge separation efficiency and charge transfer ability, and depressed effectively h^+/e^- recombination. The high-sensitive detection was achieved and benefited from the specific recognition between CD95 antibody and FLS cell. The developed ultrasensitive and stable biosensor would provide good detection for FLS cell and other analyses.

Acknowledgments

This research was supported by National Natural Science Foundation of China (Nos. 21175057, 21375047, 21377046, 21405059, 21575050 and 21505051), the Science and Technology Development Plan of Shandong Province (No. 2014GSF120004), the Special Project for Independent Innovation and Achievements Transformation of Shandong Province (No. 2014ZZCX05101), the Technology Research Project of Shandong Provincial Education Department (J15LC07), Taishan Scholar Professorship of Shandong Province and UJN (No. ts20130937).

Appendix A. Supplementary material

Supplementary data associated with this article can be found in the online version at http://dx.doi.org/10.1016/j.bios.2015.09.047.

References

Ahmad, R., Tripathy, N., Hahn, Y., 2014. Highly sensitive hydrazine chemical sensor based on ZnO nanorods field-effect transistor. Chem. Commun. 50 (15), 1890–1893.
Ball, J.M., Lee, M.M., Hey, A., Snaith, H.J., 2013. Low-temperature processed meso-superstructured to thin-film perovskite solar cells. Energy Environ. Sci. 6 (6), 1739–1743.
Burschka, J., Pellet, N., Moon, S.J., Humphry-Baker, R., Gao, P., Nazeeruddin, M.K., Gratzel, M., 2013. Sequential deposition as a route to high-performance perovskite-sensitized solar cells. Nature 499 (7458), 316–319.
Chang, H., Sun, Z., Ho, K.Y., Tao, X., Yan, F., Kwok, W., Zheng, Z., 2011. A highly sensitive ultraviolet sensor based on a facile in situ solution-grown ZnO nanorod/graphene heterostructure. Nanoscale 3 (1), 258–264.
Chen, Q., Ai, S., Zhu, X., Yin, H., Ma, Q., Qiu, Y., 2009. A nitrite biosensor based on the immobilization of Cytochrome c on multi-walled carbon nanotubes–PAMAM–chitosan nanocomposite modified glass carbon electrode. Biosens. Bioelectron. 24 (10), 2991–2996.
Cui, L., Wu, J., Ju, H., 2015. Electrochemical sensing of heavy metal ions with inorganic, organic and bio-materials. Biosens. Bioelectron 63 (0), 276–286.
Dong, X., Su, Y., Geng, H., Li, Z., Yang, C., Li, X., Zhang, Y., 2014. Fast one-step synthesis of N-doped carbon dots by pyrolyzing ethanolamine. J. Mater. Chem. C 2 (36), 7477–7481.
Gao, P., Ma, H., Yang, J., Wu, D., Zhang, Y., Du, B., Fan, D., Wei, Q., 2015. Anatase TiO_2 based photoelectrochemical sensor for the sensitive determination of dopamine under visible light irradiation. New J. Chem. 39 (2), 1483–1487.
Gu, B., Xu, C., Yang, C., Liu, S., Wang, M., 2011. ZnO quantum dot labeled

immunosensor for carbohydrate antigen 19-9. Biosens. Bioelectron. 26 (5), 2720–2723.
Gupta, V., Chaudhary, N., Srivastava, R., Sharma, G.D., Bhardwaj, R., Chand, S., 2011. Luminscent graphene quantum dots for organic photovoltaic devices. J. Am. Chem. Soc. 133 (26), 9960–9963.
Han, T., Yan, T., Li, Y., Cao, W., Pang, X., Huang, Q., Wei, Q., 2015. Eco-friendly synthesis of electrochemiluminescent nitrogen-doped carbon quantum dots from diethylene triamine pentacetate and their application for protein detection. Carbon 91, 144–152.
Hodes, G., 2013. Perovskite-based solar cells. Science 342 (6156), 317–318.
Hou, J., Dong, J., Zhu, H., Teng, X., Ai, S., Mang, M., 2015. A simple and sensitive fluorescent sensor for methyl parathion based on L-tyrosine methyl ester functionalized carbon dots. Biosens. Bioelectron. 68 (0), 20–26.
Jiang, D., Hao, Y., Shen, R., Ghazarian, S., Ramos, A., Zhou, F., 2013. Effective Blockage of the Interfacial Recombination Process at TiO_2 Nanowire Array Electrodes in Dye-Sensitized Solar Cells. ACS Appl. Mater. Interfaces 5 (22), 11906–11912.
Kim, H.S., Lee, J.W., Yantara, N., Boix, P.P., Kulkarni, S.A., Mhaisalkar, S., Gratzel, M., Park, N.G., 2013. High efficiency solid-state sensitized solar cell-based on submicrometer rutile TiO_2 nanorod and $CH_3NH_3PbI_3$ perovskite sensitizer. Nano Lett. 13 (6), 2412–2417.
Lee, M.M., Teuscher, J., Miyasaka, T., Murakami, T.N., Snaith, H.J., 2012. Efficient hybrid solar cells based on meso-superstructured organometal halide perovskites. Science 338 (6107), 643–647.
Li, H., Liu, R., Lian, S., Liu, Y., Huang, H., Kang, Z., 2013. Near-infrared light controlled photocatalytic activity of carbon quantum dots for highly selective oxidation reaction. Nanoscale 5 (8), 3289–3297.
Liu, C., Qiu, Z., Meng, W., Chen, J., Qi, J., Dong, C., Wang, M., 2015. Effects of interfacial characteristics on photovoltaic performance in $CH_3NH_3PbBr_3$-based bulk perovskite solar cells with core/shell nanoarray as electron transporter. Nano Energy 12, 59–68.
Matsuzawa, M., Kobayashi, K., Sugioka, K., Knoll, W., 1998. A biocompatible interface for the geometrical guidance of central neurons in vitro. J. Colloid Interface Sci. 202 (2), 213–221.
Narayanan, R., Deepa, M., Srivastava, A.K., 2013. Förster resonance energy transfer and carbon dots enhance light harvesting in a solid-state quantum dot solar cell. J. Mater. Chem. A 1 (12), 3907–3918.
Pandey, S., Thakur, M., Mewada, A., Anjarlekar, D., Mishra, N., Sharon, M., 2013. Carbon dots functionalized gold nanorod mediated delivery of doxorubicin: trifunctional nano-worms for drug delivery, photothermal therapy and bioimaging. J. Mater. Chem. B 1 (38), 4972–4982.
Pang, X., Pan, J., Gao, P., Wang, Y., Wang, L., Du, B., Wei, Q., 2015a. A visible light induced photoelectrochemical aptsensor constructed by aligned ZnO@CdTe core shell nanocable arrays/carboxylated g-C_3N_4 for the detection of Proprotein convertase subtilisin/kexin type 6 gene. Biosens. Bioelectron. 74, 49–58.
Pang, X., Pan, J., Wang, L., Ren, W., Gao, P., Wei, Q., Du, B., 2015b. CdSe quantum dot-functionalized TiO_2 nanohybrids as a visible light induced photoelectrochemical platform for the detection of proprotein convertase subtilisin/kexin type 6. Biosens. Bioelectron. 71, 88–97.
Peng, J., Gao, W., Gupta, B.K., Liu, Z., Romero-Aburto, R., Ge, L., Song, L., Alemany, L. B., Zhan, X., Gao, G., 2012. Graphene quantum dots derived from carbon fibers. Nano Lett. 12 (2), 844–849.
Sokka, T., 2003. Work disability in early rheumatoid arthritis. Clin. Exp. Rheumatol. 21 (5), S71–S74.
Stoumpos, C.C., Malliakas, C.D., Kanatzidis, M.G., 2013. Semiconducting tin and lead iodide perovskites with organic cations: phase transitions, high mobilities, and near-infrared photoluminescent properties. Inorg. chem. 52 (15), 9019–9038.
Sun, B., Chen, L., Xu, Y., Liu, M., Yin, H., Ai, S., 2014a. Ultrasensitive photoelectrochemical immunoassay of indole-3-acetic acid based on the MPA modified CdS/RGO nanocomposites decorated ITO electrode. Biosens. Bioelectron. 51 (0), 164–169.
Sun, B., Qiao, F., Chen, L., Zhao, Z., Yin, H., Ai, S., 2014b. Effective signal-on photoelectrochemical immunoassay of subgroup J avian leukosis virus based on Bi_2S_3 nanorods as photosensitizer and in situ generated ascorbic acid for electron donating. Biosens. Bioelectron. 54 (0), 237–243.
Sun, B., Zhang, K., Chen, L., Guo, L., Ai, S., 2013. A novel photoelectrochemical sensor based on PPIX-functionalized WO_3–rGO nanohybrid-decorated ITO electrode for detecting cysteine. Biosens. Bioelectron. 44 (0), 48–51.
Sun, M., Ma, X., Chen, X., Sun, Y., Cui, X., Lin, Y., 2014c. A nanocomposite of carbon quantum dots and TiO_2 nanotube arrays: enhancing photoelectrochemical and photocatalytic properties. RSC Adv. 4 (3), 1120–1127.
Tsai, T., Wang, S., Chen, S., 2011. Electrodeposited indigotetrasulfonate film onto glutaraldehyde-cross-linked poly-L-lysine modified glassy carbon electrode for detection of dissolved oxygen. J. Electroanal. Chem. 659 (1), 69–75.
Van Berkel, G.J., Zhou, F., 1995. Characterization of an electrospray ion source as a controlled-current electrolytic cell. Anal. Chem. 67 (17), 2916–2923.
Wang, F., Wang, L., Jiang, H., Chang, X., Pan, J., 2014. Inhibition of PCSK6 may play a protective role in the development of rheumatoid arthritis. J. Rheumatol. . http://dx.doi.org/10.3899/jrheum.140435
Wang, J., Sun, X., Yang, Y., Huang, H., Lee, Y., Tan, O., Vayssieres, L., 2006. Hydrothermally grown oriented ZnO nanorod arrays for gas sensing applications. Nanotechnology 17 (19), 4995.
Wang, X., Chen, L., Su, X., Ai, S., 2013. Electrochemical immunosensor with graphene quantum dots and apoferritin-encapsulated Cu nanoparticles double-assisted signal amplification for detection of avian leukosis virus subgroup. J. Biosens. Bioelectron. 47 (0), 171–177.
Wang, X., Zhu, H., Xu, Y., Wang, H., Tao, Y., Hark, S., Xiao, X., Li, Q., 2010. Aligned ZnO/CdTe core – shell nanocable arrays on indium tin oxide: synthesis and photoelectrochemical properties. ACS Nano 4 (6), 3302–3308.
Wang, Z.L., Song, J., 2006. Piezoelectric nanogenerators based on zinc oxide nanowire arrays. Science 312 (5771), 242–246.
Weng, C.-I., Chang, H.-T., Lin, C.-H., Shen, Y.-W., Unnikrishnan, B., Li, Y.-J., Huang, C.-C., 2015. One-step synthesis of biofunctional carbon quantum dots for bacterial labeling. Biosens. Bioelectron. 68 (0), 1–6.
Xu, Q., Wang, L., Lei, J., Deng, S., Ju, H., 2013. Platinum nanodendrite functionalized graphene nanosheets as a non-enzymatic label for electrochemical immunosensing. J. Mater. Chem. B 1 (39), 5347–5352.
Yang, S., Wang, X., Wang, H., Lu, F., Luo, P.G., Cao, L., Meziani, M.J., Liu, J., Liu, Y., Chen, M., 2009. Carbon dots as nontoxic and high-performance fluorescence imaging agents. J. Phys. Chem. C 113 (42), 18110–18114.
Yin, H., Sun, B., Dong, L., Li, B., Zhou, Y., Ai, S., 2015. A signal “on” photoelectrochemical biosensor for assay of protein kinase activity and its inhibitor based on graphite-like carbon nitride, Phos-tag and alkaline phosphatase. Biosens. Bioelectron. 64 (0), 462–468.
Zang, Y., Lei, J., Hao, Q., Ju, H., 2014a. “Signal-On” Photoelectrochemical Sensing Strategy Based on Target-Dependent Aptamer Conformational Conversion for Selective Detection of Lead(II) Ion. ACS Appl. Mater. Interfaces 6 (18), 15991–15997.
Zang, Y., Lei, J., Zhang, L., Ju, H., 2014b. In Situ Generation of Electron Acceptor for Photoelectrochemical Biosensing via Hemin-Mediated Catalytic Reaction. Anal. Chem. 86 (24), 12362–12368.
Zhang, M., Liu, H., Chen, L., Yan, M., Ge, L., Ge, S., Yu, J., 2013. A disposable electrochemiluminescence device for ultrasensitive monitoring of K562 leukemia cells based on aptamers and ZnO@carbon quantum dots. Biosens. Bioelectron. 49 (0), 79–85.
Zhang, X., Liu, M., Liu, H., Zhang, S., 2014. Low-toxic Ag_2S quantum dots for photoelectrochemical detection glucose and cancer cells. Biosens. Bioelectron. 56 (0), 307–312.
Zhao, Y., Qi, L., Chen, F., Fan, C., 2013. Highly sensitive detection of telomerase activity in tumor cells by cascade isothermal signal amplification based on three-way junction and base-stacking hybridization. Biosens. Bioelectron. 41, 764–770.
Zhou, F., Van Berkel, G.J., 1995. Electrochemistry combined online with electrospray mass spectrometry. Anal. Chem. 67 (20), 3643–3649.